DOI: 10.58895/ksp/1000128686-11 erschienen in:
OCM 2021 - 5th International Conference on Optical Characterization of Materials, March 17th – 18th, 2021, Karlsruhe, Germany : Conference Proceedings
DOI: 10.58895/ksp/1000128686 | https://www.ksp.kit.edu/site/books/m/10.58895/ksp/1000128686/

Vessel extraction from breast MRI

Marco Gierlinger, Dinah Brandner, and Bernhard G. Zagar

Johannes Kepler University Linz, Institute for Measurement Technology, Altenberger Straße 69, AT-4040 Linz

Abstract We present an extension of the previous work, where a multi-seed region growing (MSRG) algorithm was shown, that extracts segments from breast MRI. The algorithm of our extended work filters elongated segments from the segments derived by the MSRG algorithm to obtain vessel-like structures. This filter is a skeletonization-like algorithm that collects useful information about the segments' thickness, length, etc. A model is shown that scans through the solution space of the MSRG algorithm by adjusting its parameters and by providing shape information for the filter. We further elaborate on the usefulness of the algorithm to assist medical experts in their diagnosis of diseases relevant to angiography.

Keywords Feature extraction, breast MRI, region-based, image segmentation

1 Introduction

Magnet resonance (MR) angiography is a diagnostic tool to depict vessels, e.g. blood vessels. Also, potential malignant masses like cancer can be analyzed, since the spread of cancer is supported by excreting angiogenesis factor to prompt vessel growth into the mass to provide nutrients and oxygen [1]. Information about location, size and morphology of vessels may provide clinicians with useful information before surgery during e.g. a neoadjuvant therapy. Blood vessels in breast MRI are determined subjectively by radiologists, which is considered as the gold standard as research shows [2,3]. Rarely accessible data-sets and their expensive annotation by experts hinder the progress of vessel extraction in medical fields with deep-learning [4]. In recent years,

many researchers were motivated to provide clinicians with useful algorithms for vessel segmentation for medical diagnostics [5].

In previous work, we developed a fast multi-seed region growing (MSRG) algorithm [6], that is capable of extracting homogeneous regions even in images exhibiting noise artefacts. While the algorithm is still in active development, it has shown promising results on which we rely on in this current contribution. The algorithm generates a finite two-dimensional solution space of extracted homogeneous regions from a given input image. We extend the previous work with a skeletonization-like algorithm that is capable of filtering elongated segments from this solution space.

In Section 2, the algorithm of the previous work is explained in detail. The subsequent sections will describe the skeletonization-like algorithm and show the results of allegedly extracted vessels.

2 Previous Work

The multi-seed region growing (MSRG) algorithm is described for n-bit RGB images in $\mathbb{N}_0^{w\times h\times 3}$ as follows: Multiple seeds are employed and aligned as grid with a user-defined width u and height v with $u, v \in \mathbb{N}$, $u \leq w$ and $v \leq h$ as schematically depicted in red ($u = v = 3$) on the blue pane of Fig. 2.1. The algorithm walks through pixel space in an 8-adjacency flood-fill manner independently for each of the k seeds as follows: Let $\vec{p} \in \mathbb{N}_0^5 = (p_0, p_1, p_R, p_G, p_B)$ be a pixel, where (p_0, p_1) is its position in pixel space and let $I_R(\vec{p}) = p_R$, $I_G(\vec{p}) = p_G$, and $I_B(\vec{p}) = p_B$ be its intensity values. A bucket queue is used to hold data objects $(\vec{p}, q)$, where $q \in \mathbb{N}_0$ with $q < 2^n$ is the bucket's index. Initially, the queue is filled with the seed only, which is a single pixel only. An iteration i is initiated by polling a bucket B_i. $\forall \vec{a} \in B_i \; \forall \vec{b} \in N'(\vec{a})$, a cost function $\delta_f : (\vec{a}, \vec{b}) \mapsto \{r \in \mathbb{N}_0 \mid r < 2^n\}$ is applied, where $N'(\vec{a})$ denotes all non-visited neighbors of $\vec{a}$. Cost function δ_f is defined as:

$$\delta_f(\vec{a}, \vec{b}) = \left\lfloor \sqrt{\frac{(I_R(\vec{a}) - I_R(\vec{b}))^2 + (I_G(\vec{a}) - I_G(\vec{b}))^2 + (I_B(\vec{a}) - I_B(\vec{b}))^2}{3}} \right\rfloor. \tag{2.1}$$

At the end of an iteration, each result is added to the queue as $(\vec{b}, \delta_f(\vec{a}, \vec{b}))$.

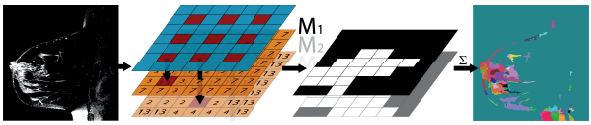

Figure 2.1: MSRG applied to a single slice of breast MRI dataset [7].

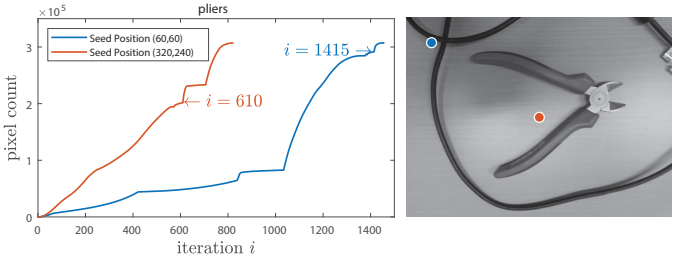

Figure 2.2: Left: Cumulative frequency of number of assigned pixels m_i on 'pliers' image with $(w, h) = (640, 480)$ and largest step $m_{\max}$ is found at highlighted iteration i. Right: Image with arbitrary seed positions indicated.

2.1 Heuristic

Additionally, the number of newly assigned pixels m_i is tracked for each iteration i. A map $M_s \in \mathbb{N}_0^{w \times h}$, drawn as an orange pane in Fig. 2.1, is used for the s^{th} of k seeds and every $r_{a_0,a_1} \in M_s$, where (a_0, a_1) is the position of $\vec{a}$, is set to $m_{\max}(i) = \max(m_0, m_1, ..., m_i)$ at iteration i. Finally, when the queue is empty, i.e. every pixel was visited, M_s is converted into a binary map by

$$r \in M_s = \begin{cases} 0 & r < m_{\max}(i) \\ 1 & \text{otherwise} \end{cases} \tag{2.2}$$

Then, all k binary maps are added up elementwise to $\sum_{s=1}^{k} M_s$, and normalized to the range from zero to $2^n - 1$ to suppress regions that

occur less often than others. An example is highlighted in Fig. 2.1 (right) with random colors assigned for regions containing the same numerical value. Growth is depicted in Fig. 2.2 and Fig. 2.3 for two arbitrary seed positions.

Furthermore, an image quantization factor $g \in \mathbb{R}$ with $0 < g \leq 1$ is used to decrease the image's bit depth as a preprocessing step. A user can tune the grid size (u, v), i.e. the density of dispersed seeds, and image quantization factor g until a suitable solution is found as shown in Fig. 2.4.

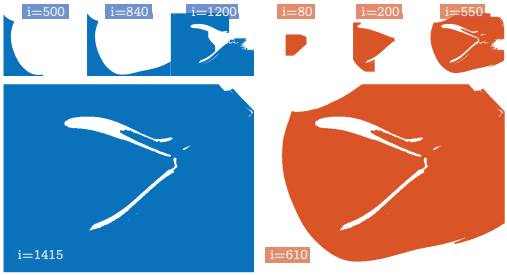

Figure 2.3: Growth of blue seed at $(60, 60)$ and orange seed at $(320, 240)$ on 'pliers'.

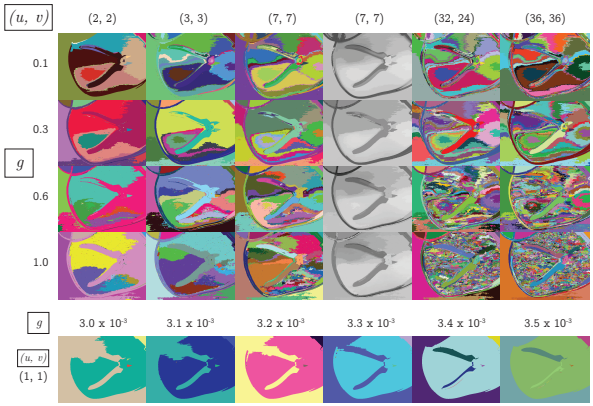

Figure 2.4: Solution space of MSRG [6].

3 Proposed Method

In this section we initially detail an algorithm that filters elongated segments from the result set of the multi-seed region growing (MSRG) algorithm. Furthermore, in the second subsection, a model is depicted to show how these two algorithms interact to obtain vessel-like structures from an input breast MRI stack. The stack is defined as follows: Let S_i be the i^{th} image on the breast MRI stack, that is an 8-bit grayscale image, we define C_i as an RGB image, that is composed of S_i as red channel, S_{i+1} as green channel and S_{i+2} as blue channel. For example, the top of the second stack from left (C_{24}) in Fig. 3.1 shows such an 8-bit 256×256 RGB image as one of 34 possible slices.

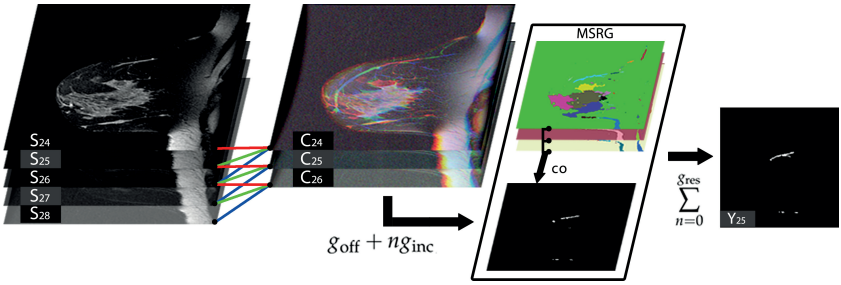

Figure 3.1: From left to right: Five of a set of 36 Breast MRI slices of a single session $\rightarrow$ RGB image composited by three grayscale images from the left stack $\rightarrow$ Filtered MSRG algorithm $\text{fi}(C, g_{\text{off}} + n \cdot g_{\text{inc}}) \rightarrow$ Result stack showing a single result slice.

3.1 Algorithm

Elongated vessel-like segments are filtered out from the set of segments derived by the MSRG. We apply a skeletonization-like algorithm $\text{sk}(\text{msrg}(C, g, u, v)) = M_{\text{sk}}$, where C is an arbitrary RGB image and g, u, v the other MSRG input parameters as described in the previous section. Result M_{sk} is a binary map containing the filtered segments. The algorithm $\text{sk}(\text{msrg}(C, g, u, v))$ is described for a single segment of the MSRG result set as follows:

Initially, we select a random pixel $\vec{p}$ from given segment A and 8-adjacently flood-fill until every pixel has been 'filled'. Let

$N(\vec{p})$ be the set of adjacent filled pixels of $\vec{p}$ in pixel space of A. Each iteration, we prioritize from the set of potential new pixels $N(A) = \{r \in A \mid \neg\text{isfilled}(r) \wedge N(r) \neq \varnothing\}$ the subset $N_{\max}(A) \subseteq N(A)$, defined as the largest group of adjacent pixels as highlighted in Fig. 3.2 left.

This rule leads to a fast method such that the segment is flood-filled nearly homogeneously along an elongated segment as shown in Fig. 3.2 right. Each iteration and until every pixel has been examined, we derive an updated set of $N_{\max}(A)$. We use this set for statistical analysis: E.g., $|N_{\max}(A)|$ gives a rough estimation of the thickness of an elongated shape. This statistical information is useful to filter out segments that are too short, too thick, or have a too large variance in thickness or intensity along the potential vessel or along its cross section. With this filter, the number of parameters increases but the parameters could be adjusted by medical experts to fit the realistic requirements of the vessels in question.

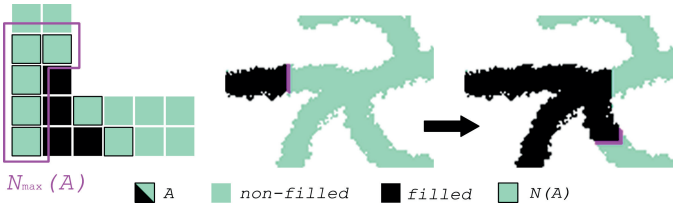

Figure 3.2: A Flood-fill algorithm that promotes nearly homogeneous flooding by prioritizing the largest adjacent group $N_{\max}(A) \subseteq N(A)$.

3.2 Model

We generate with the MSRG a one-dimensional solution space: The seed grid size (u, v) is set to $(4, 4)$, i.e. we select a column as shown in Fig. 2.4. These values are selected based on user experience with the MSRG. We define within this subsection the filtered MSRG algorithm $\text{fi}(C, g) = \text{sk}(\text{msrg}(C, g, 4, 4))$, where $\text{sk}(\text{msrg}(C, g, 4, 4))$ denotes the filter algorithm from the previous subsection. The algorithm $\text{fi}(C, g)$ is applied to RGB (3 channels) image $C \in \mathbb{N}_0^{w \times h \times 3}$ with image width w and image height h and results in a binary map $M_{\text{fi}} \in \mathbb{N}_0^{w \times h}$. The

image quantization factor $g \in \mathbb{R}$ with $0 < g \leq 1$ is now the only parameter that influences the result.

To keep the computation time low, we do not iterate over all possible values of the image quantization factor g. We limit the range from g_{off} to $g_{\text{off}} + g_{\text{inc}} \cdot g_{\text{res}}$, where g_{off} denotes the lower bound, g_{res} the resolution, and $g_{\text{off}} + g_{\text{inc}} \cdot g_{\text{res}}$ the upper bound of the dimension. Again, the values are selected based on user experience of the MSRG and should be selected such that the desired features are found within these bounds.

The model is schematically depicted in Fig. 3.1. The results are binary images with elongated structures that potentially reveal vessels. Formally, we generate a result stack (see Fig. 3.1 right) for all $j \in \mathbb{N}$ with $1 < j \leq (\text{MRI stack size} - 3)$, defined as:

$$Y_j = \sum_{n=0}^{g_{\text{res}}} \text{co}(C_{j-1}, C_j, C_{j+1}, g_{\text{off}} + n \cdot g_{\text{inc}}) \tag{3.1}$$

where $\text{co}(R_1, R_2, R_3, g)$ returns a single binary map that is composed of the union of the two adjacent slice pairs. Formally,

$$\text{co}(R_1, R_2, R_3, g) = \text{fi}(R_1, g) \wedge \text{fi}(R_2, g) \vee \text{fi}(R_2, g) \wedge \text{fi}(R_3, g) \tag{3.2}$$

where $\wedge$ and $\vee$ denote element-wise binary operators. Finally, as a post processing step, we set

$$r \in Y_j = \begin{cases} 0 & r < t \\ 1 & \text{otherwise} \end{cases} \tag{3.3}$$

where t is a user-defined threshold.

With this technique, it is possible to differ the contours of the skin from elongated segments that are within the region of interest. We assume that the color gradient more likely varies along the cross section as shown in Fig. 3.3. This can be detected by the algorithm of the previous subsection by statistical analysis of $N_{\max}(A)$.

4 Results and Evaluation

We apply the proposed method of the previous section to two different breast MRI stacks that were acquired from the same patient (and same

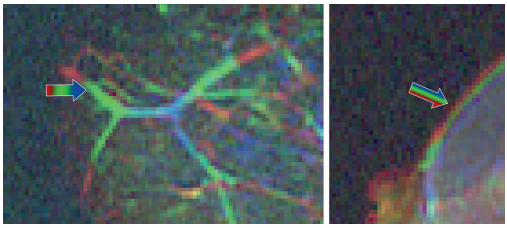

Figure 3.3: Left: A potential vessel with color gradient varying lengthwise. Right: Breast contour with color gradient varying along the cross section.

breast) during two sessions. Several weeks lay between these two sessions. Algorithm parameters are set for both stacks equally. The result is shown in Fig. 4.1 for four adjacent slices of each result stack. Slices of these two stacks are shifted such that they roughly match each other from column to column in Fig. 4.1. We derive similar results for both stacks, although the region of interest is shaped differently as seen in the two RGB images of Fig. 4.1. However, these binary results do not cover all elongated structures as visible in the RGB images. A better strategy is required to efficiently look for elongated segments in the solution space of the MSRG algorithm to derive more results. Also, a slice represents 3 mm thickness and obviously, a much higher resolution would improve the results for thinner vessel-like structures.

Due to the breast varying in shapes in different postures, it is very challenging to detect common features, however, this method might be used for automatic image registration.

5 Conclusions

With our proposed filter and combined with the MSRG algorithm from the previous work, it seems possible to assist clinicians in detecting vessel-like segments. The employed algorithm filtered elongated structures from the solution space of the MSRG algorithm. The results seem promising, however, they could not be evaluated for the correct detection of vessels without medical expertise. Instead, the proposed method was applied to two input MRI stacks from the same patient (and same breast), that were acquired during two sessions. The evalua-

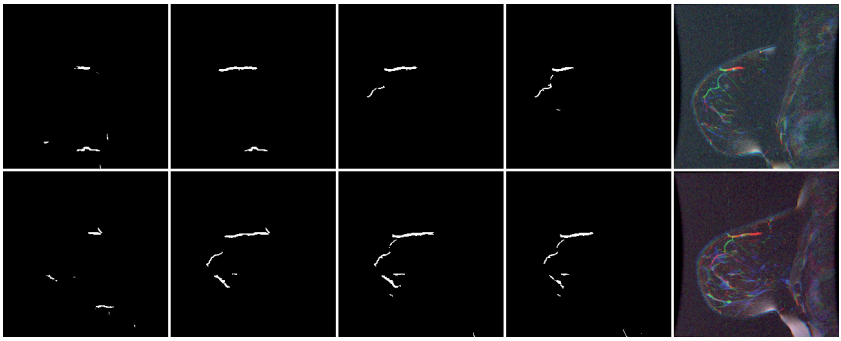

Figure 4.1: Each row contains four adjacent slices of the result stack as shown in Fig. 3.1 right. Each row's input stack (Fig. 3.1 on the left) was acquired from the same patient but several weeks lay between these sessions.

tion showed how barely the results deviate from each other. Although vessels will be positioned slightly differently between two sessions due to shaping the breast dependent on the actual posture in the MRI scanner, this method seemingly extracted similar elongated segments for both input MRI stacks. This suggests the assumption that the extracted segments are not artefacts.

Based on user experience, the solution space of the MSRG algorithm was searched through. Due to the complexity and computation time, it is impractical to search through the whole solution space. It is required to adjust the MSRG parameters accordingly, however, the MSRG algorithm is not guaranteed to be complete. Further investigations are required for more efficient search strategies.

Acknowledgement

This work has been supported by the LCM K2 Center within the framework of the Austrian COMET-K2 Programme.

References

1. Nishida N., Yano H., Nishida T., Kamura T., Kojiro M., "Angiogenesis in cancer." *Vasc. Health Risk Manag. 2, 213–219*, 2006.
2. Kahala G., Sklair M., Spitzer H., "Multi-scale blood vessel detection and segmentation in breast mris." *Journal of Medical and Biological Engineering volume 39, 424–430*, 2019.
3. Lin M., Chen J.H., Nie K., Chang D., Nalcioglu O., Su M.Y., "Algorithm-based method for detection of blood vessels in breast mri for development of computer-aided diagnosis." *J Magn Reson Imaging 2009; 30: 817-824*, 2009.
4. Lundervold A.S., Lundervold A., "An overview of deep learning in medical imaging focusing on mri." *Zeitschrift für Medizinische Physik, 29 (2) (2019), pp. 102-127.*, 2019.
5. Moccia S., De Momi E., El Hadji S., Mattos L.S., "Blood vessel segmentation algorithms review of methods, datasets and evaluation metrics." *Comput. Methods Programs Biomed., 158 (2018), pp. 71-91*, 2018.
6. Gierlinger M., Brandner D., Zagar B., "Multi-seed region growing algorithm for medical image segmentation." *M. Heizmann and T. Längle: Proceedings of FORUM BILDVERARBEITUNG 2020, KIT Scientific Publishing, Seite(n) 267 - 278.*, 2020.
7. D. Newitt, N. Hylton, on behalf of the I-SPY 1 Network and ACRIN 6657 Trial Team, "Multi-center breast dce-mri data and segmentations from patients in the i-spy 1/acrin 6657 trials." *The Cancer Imaging Archive. http://doi.org/10.7937/K9/TCIA.2016.HdHpgJLK*, 2016.